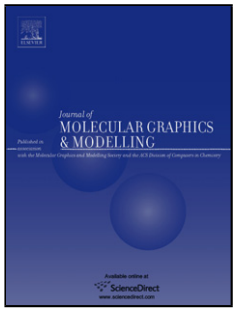

Title: Association of the anti-tuberculosis drug rifampicin with a PAMAM dendrimer

Author: Reinaldo G. Bellini Ana P. Guimarães Marco A.C. Pacheco Douglas M. Dias Vanessa R. Furtado Ricardo B. de Alencastro Bruno A.C. Horta

PII: S1093-3263(15)30002-4
DOI: http://dx.doi.org/doi:10.1016/j.jmgm.2015.05.012
Reference: JMG 6552

To appear in: *Journal of Molecular Graphics and Modelling*

Received date: 8-1-2015
Revised date: 3-5-2015
Accepted date: 22-5-2015

Please cite this article as: R.G. Bellini, A.P. Guimaraes, M.A.C. Pacheco, D.M. Dias, V.R. Furtado, R.B. de Alencastro, B.A.C. Horta, Association of the anti-tuberculosis drug rifampicin with a PAMAM dendrimer, *Journal of Molecular Graphics and Modelling* (2015), http://dx.doi.org/10.1016/j.jmgm.2015.05.012

Association of the anti-tuberculosis drug rifampicin with a PAMAM dendrimer

Reinaldo G. Bellini[a], Ana P. Guimarães[b], Marco A. C. Pacheco[a], Douglas M. Dias[a], Vanessa R. Furtado[c], Ricardo B. de Alencastro[c], Bruno A. C. Horta[c]

Corresponding address:
Instituto de Química - Universidade Federal do Rio de Janeiro,
Av. Athos da Silveira Ramos, 149 Centro de Tecnologia, Bloco A, Sala 609 21941-909
Cidade Universitária, Rio de Janeiro - RJ, Brazil
Phone: +55 21 3938 7132

[a]*Departamento de Engenharia Elétrica, PUC-Rio, Rio de Janeiro, Brazil*
[b]*Departamento de Química, Universidade Federal de Viçosa, Viçosa, Brazil*
[c]*Instituto de Química, Universidade Federal do Rio de Janeiro, Rio de Janeiro, Brazil*

Abstract

The association of the anti-tuberculosis drug rifampicin (RIF) with a 4^{th}-generation poly(amidoamine) (G4-PAMAM) dendrimer was investigated by means of molecular dynamics simulations. The RIF load capacity was estimated to be around 20 RIF per G4-PAMAM at neutral pH. The complex formed by 20 RIF molecules and the dendrimer (RIF_{20}-PAMAM) was subjected to 100 ns molecular dynamics (MD) simulations at two different pH conditions (neutral and acidic). The complex was found to be significantly more stable in the simulation at neutral pH compared to the simulation at low pH in which the RIF molecules were rapidly and almost simultaneously expelled to the solvent bulk. The high stability of the RIF-PAMAM complex

Email address: bruno@iq.ufrj.br (Bruno A. C. Horta)

under physiological pH and the rapid release of RIF molecules under acidic medium provide an interesting switch for drug targeting since the *Mycobacterium* resides within acidic domains of the macrophage. Altogether, these results suggest that, at least in terms of stability and pH-dependent release, PAMAM-like dendrimers may be considered suitable drug delivery systems for RIF and derivatives.

Keywords: Computer simulation, molecular dynamics, dendrimer, PAMAM, rifampicin, drug delivery

1. Introduction

Tuberculosis (TB) is an infectious disease caused by the bacillus *Mycobacterium tuberculosis* (also known as Koch bacillus) that survives and replicates within human alveolar macrophages. It typically affects the lungs (pulmonary TB) but can also extend to other organs (extrapulmonary TB). It is a common cause of death among HIV-positive patients.[1] According to the latest report of the World Health Organization (WHO), 8.6 million new TB cases together with 1.3 million deaths by TB were reported in 2012.[2] Therefore, TB remains a major global health problem.

Typical TB treatment follows a six-month administration of a cocktail consisting of four antibiotics: rifampicin, isoniazid, pyrazinamide and ethambutol.[3, 4] Rifampicin (RIF) (Figure 1a) is reported as an essential component of the cocktail.[5, 6] Its mechanism of action is related to the inhibition of the β subunit of the bacterial RNA polymerase, thus inhibiting gene transcription.[6] However, several side effects have been associated with this drug such as nausea, vomiting, weight loss, hepatotoxicity, skin and

gastrointestinal adverse reactions and immune responses.[6–8]. As a consequence of the several side effects along with the lengthy treatment period, there is a low adherence to drug administration schedules, which facilitates the development of multi-drug resistant tuberculosis.[9]

Several side effects of RIF are related to its pharmacokinetics, mainly to its low solubility in water.[10–12] Under gastric conditions, RIF suffers hydrolysis leading to even less soluble compounds such as 3-formyl-rifampicin. Moreover, RIF is known to interact with isoniazid leading to an insoluble hydrazone.[13, 14]

In order to improve the bioavailability of RIF and the other tuberculostatic drugs, several research groups have been developing drug delivery systems (DDS).[12] Suggested formulations involve hydrosoluble polymers,[15–19] solid dispersions,[20] microparticles,[9] liposomes, [21, 22] inclusion complexes[23, 24] and dendrimers[25]. Ideally, a DDS would transport the active compounds to their targets, reducing the therapeutic dosage while keeping the desired drug level for a long period of time, minimizing adverse effects and simplifying the treatment. Moreover, the fact that the *M. tuberculosis* resides within the phagosome compartment of the macrophage, which exhibits a pH around 4.5, opens the possibility for a pH-based vectorization of drugs using a DDS which is able to retain the active compound under physiological pH (~ 7.4) and effectively release them under an acidic environment (pH ~ 4.5, in this case).

Dendrimers are highly branched artificial molecules that are designed in such a way that a core moiety serves as a platform for the binding of repeating molecular groups, leading to a shell of these groups around the central

moiety. For each new shell, it is said that a dendrimer has achieved a new "generation". Its diameter can be controlled so as to achieve the desired properties, which usually happens around a few nanometers. Three different regions can be identified in a dendrimer structure: (*i*) the encapsulating core, which can harbour chemical species due to the microenvironment created by the branches; (*ii*) the intermediate region, created within the space between the flexible branches, which provides a refuge from the outside environment; (*iii*) the multivalent surface, which can accommodate a large number of functional groups that interact with the environment and define the macroscopic properties of the dendrimer.[26] Due to their structural possibilities and versatility, dendrimers have been studied in the context of materials,[27–29] sensors,[30–32] gene therapy,[33] contrast agents for magnetic resonance imaging,[34, 35] crystallization,[36, 37] solid-phase chemistry,[38] catalysis,[39–42] cosmetics[43] and other fields. Dendrimers are also very promising DDS systems due to their high drug-loading capacity, controllable load and release due to significant structural changes upon environmental changes (*e.g.* conformation is usually strongly dependent on pH conditions), and surface functional groups that could possibly discriminate biological targets and enhance drug solubility.[44–52]

The poly(amidoamine) (PAMAM) dendrimers are the first and most extensively studied family of dendrimers.[44] Figure 1b depicts the three-dimensional structure of a model of a 4^{th}-generation PAMAM (G4-PAMAM). In addition to their ability to carry a considerable load of small molecules, they have been shown to incorporate into biomembranes and cells and are thus capable of delivering small active compounds in the intracellular region.[53–

57]

There have been increasing efforts of using computer simulations for understanding and predicting molecular properties of dendrimers as well as their assembly with guest molecules and with biomacromolecules.[55, 58–67] Molecular dynamics (MD) simulation, which is a powerful tool for investigating properties of molecular systems relevant in physics, chemistry and biology[68–71], has been the major technique used in this respect. In terms of the drug-dendrimer association phenomena, MD simulations have been used to study the association of ibuprofen with G3-PAMAM,[55] nicotinic acid with G3-PAMAM,[57] four drug molecules (salicylic acid, L-alanine, primidone and phenylbutazone) with G5-PAMAM,[72] three drug molecules (famotidine, indomethacin and phenylbutazone) with poly(propylene imine) (PPI) dendrimers[73] and piroxicam with G3-PAMAM.[74]

The main goal of the present work is to study the stability of the RIF-PAMAM complexes under different pH conditions using MD simulations in order to evaluate the suitability of PAMAM as a pH-based DDS for RIF molecules. As a first step, the drug-load capacity was estimated to be ∼20 RIF molecules per G4-PAMAM. MD simulations were subsequently carried out for a free 4^{th}-generation (G4) PAMAM in solution and for the complex involving the G4-PAMAM with 20 RIF molecules (RIF_{20}-PAMAM) at two different protonation states: one mimicking the situation at physiological pH and the other mimicking the situation at the acidic pH environment of the interior of a macrophage.

2. Methodology

2.1. Experimental determination of RIF/PAMAM stoichiometry

A solution of RIF and G4-PAMAM (50:1 molar ratio) in methanol was stirred for 12 hours, under a nitrogen atmosphere. After complete removal of the methanol by distillation under reduced pressure, the residue was dissolved in 200 μL of distilled water and submitted to centrifuge ultra-filtration (6499 rpm) in Microcon YM-3 membrane (Cutoff: 3000 NMWL). The retentate was washed twice with 200 μL portions of distilled water. The filtrates were combined and the encapsulated RIF was indirectly quantified by measuring the concentration of the free RIF molecules with UV analysis (475 nm). The spectra were acquired by using a Varian Cary (1E) UV-visible spectrophotometer (Varian, Australia).

2.2. Generation of initial coordinates

In order to include as many RIF molecules as possible within the cavities of the G4-PAMAM dendrimer in physically reasonable configurations a computational procedure was carried out. The idea behind this procedure is to provide a realistic starting structure for the MD simulation of the complex RIF_n-PAMAM, where the subscript n denotes the number of RIF molecules within the complex. The structure of the individual RIF molecule was taken from the DrugBank.[75] The individual RIF molecules were treated as "ligands" and the PAMAM dendrimer as the "receptor" in a similar way as a conventional docking algorithm[76–79]. The main differences between the current procedure and conventional docking are: (i) the number of docked ligands, which characterizes the present method as a "multidocking" ap-

proach (*i.e.* in conventional docking only one ligand is considered); (*ii*) the lack of a grid for storing the receptor interactions (*i.e.* the interactions between all ligand sites and all receptor sites are computed) and (*iii*) active site is not predefined although a search space is restricted to regions close to the dendrimer. Only translational and rotational degrees of freedom of the RIF molecules were taken into account (rigid body) and the dendrimer was also kept rigid. In order to take into account the effects of having different dendrimer structures, the algorithm was performed multiple times for a set of time-uncorrelated dendrimer structures that were taken from a previously performed MD simulation of the PAMAM dendrimer in water. In order to guarantee that the selected dendrimer configurations were sufficiently different and at the same time representative of the conformational ensemble, an RMSD based cluster analysis was performed considering RMSD of 0.25 nm and the most populated configurations were considered. The procedure was performed for structures corresponding to the simulations of the dendrimer in neutral and low pH (see Section 2.4.1).

For each of the selected dendrimer structures, the following procedure was carried out:

1. The water molecules and counterions were removed.
2. In an iterative way, RIF molecules were inserted one by one inside the cavities of the dendrimer. This insertion was carried out by generating a configuration of a randomly oriented RIF molecule centered at the Cartesian space origin, which corresponds to the center of the dendrimer as it was previously centered in the origin. The RIF molecule was then translated by randomly choosing a new position for its center

of mass, and atom superposition was evaluated. If the RIF molecule presented any atom superposition, the procedure was repeated. In order to restrict the search space, a boundary condition was imposed so that the RIF molecules were only allowed within a given radial threshold value (R_t) calculated from the dendrimer center of geometry. In order to analyze the sensitivity of the method towards this imposed condition, three values of R_t were considered, 1.5, 2.5 and 3.5 nm. Once a reasonable (*i.e.* does not show any atom superposition) configuration was found, the procedure was repeated for the next RIF molecule until the stop condition was achieved (*i.e.* ten thousand cycles without succeeding to insert the next molecule). The saturation level found to be dependent on the value of R_t, on the dendrimer structure, on the order and position of the previous RIF molecules inserted and on the efficiency of the search algorithm.

3. The interaction energies were calculated using the Dreiding potential energy function[80] implemented in the GAUSSIAN package.[81]
4. Steps 2 and 3 were repeated 250 times and the configurations were ranked by energy and stored. This configuration set was labelled as "primary set".
5. In order to improve the sampling efficiency, 250 additional configurations were generated and labelled as "secondary set", but this time following a given type of distribution function to generate configurations in the vicinity of the ones in the primary set. The distribution functions considered were: (*i*) random distribution; (*ii*) Cauchy distribution; (*iii*) exponential distribution; (*iv*) gamma distribution; (*v*)

Laplace distribution; and (*vi*) Poisson distribution. The secondary set was generated according to each type of the corresponding function considered. Therefore, for each dendrimer configuration, 1750 configurations of RIF$_n$-PAMAM complexes were generated. (*i.e.* 250 from the primary set + 250 from the secondary set for each type of distribution function). This approach restricts the sampling to the subspace in the neighborhood of the best solutions of the primary set, since the probability of generating a configuration in the vicinity of the low energy ones is increased.

The success rate was defined as the number of times that the algorithm was able to insert a given number n of RIF molecules divided by the number of execution runs and multiplied by 100 (given in %). The success rate of the algorithm decreases with n (*i.e.* the number of times that the algorithm is able to dock 10 molecules is always greater than or equal to the number of times that the algorithm is able to dock 11 molecules). The procedure provides the success rate and the configurations achieved with all distribution types ranked by decreasing number n of RIF and by energy as outputs.

2.3. MD Simulation protocol

The MD simulations were performed using the GROMACS simulation package[82–85] together with the OPLS all-atom force field[86, 87] and the TIP3P water model.[88] The simulations were carried out under periodic boundary conditions based on cubic computational boxes. Newton's equations of motion were integrated using the leapfrog scheme[89] with a time step of 2 fs. All bond lengths were constrained using the LINCS procedure.[90]

The center of mass motion was removed every 100 ps. The simulations were performed in the NPT ensemble (constant number of particles N, pressure P, and temperature T) with a reference pressure P of 1 bar, and reference temperatures T of 310 K. The temperature was maintained by weakly coupling the solute and solvent degrees of freedom separately to temperature baths[91] at temperature T, with a relaxation time of 0.1 ps. The pressure was maintained by weakly coupling the particle coordinates and box dimensions isotropically to a pressure bath at pressure P, with a relaxation time of 0.5 ps and an isothermal compressibility of 7.513 10^{-4} (kJ mol^{-1} nm^{-3})$^{-1}$. The nonbonded interactions were computed using a lattice-sum scheme following the particle-mesh Ewald (PME) formalism,[92] with cutoff distances of 1.0 and 1.4 nm for electrostatic and Lennard-Jones interactions, respectively. Configurations were saved every 5 ps for analysis.

2.4. Simulated systems

2.4.1. PAMAM dendrimer in water

Initial G4-PAMAM dendrimer structures with protonation states appropriate for low and physiological pH were modelled using the HYPERCHEM-Professional program.[93] The protonation states were assigned according to titration experimental data of Cakara *et al.*[94]: (*i*) the G4-PAMAM dendrimer is fully unprotonated for pH above 9; (*ii*) for pH between 7 and 8, all primary amine groups can be considered protonated; (*iii*) for pH between 3 and 5, in addition to the primary amines, all tertiary amine groups can be considered protonated as well, with the possible exception of one of the two amine groups in the core region, which has a microcostant around 3.5. Based on these results, the dendrimer at physiological pH ($\sim$ 7.4) was considered

to be protonated at all primary amine sites, whereas the dendrimer at low pH ($\sim$ 4.5), which simulates the condition in the interior of the macrophage, was considered to be protonated at all primary and tertiary amine sites (including the core). These systems were labelled as PAMAM_N and PAMAM_L, where the subscripts N and L denote a structure appropriate for neutral and low pH conditions, respectively. The corresponding topologies were generated using the MKTOP program[95] and the OPLS-AA force field.[86, 87] The OPLS compatible atomic partial charges were generated following the procedure described in Ref.[96] Systems were energy minimized in vacuum using 2000 steps of the steepest descent algorithm followed by 2000 steps of the conjugate gradient algorithm. The structures PAMAM_N and PAMAM_L were solvated with 20553 and 20593 water molecules, respectively, in cubic computational boxes. In a subsequent step, systems were neutralized with an appropriate number of Cl^- ions, 64 in the case of PAMAM_N (*i.e.* only terminal amines are protonated) and 126 in the case of PAMAM_L (*i.e.* both terminal and tertiary amines are protonated). An equilibration simulation was performed in order to bring the system to the desired thermodynamic conditions and, after equilibration, each system was simulated for 58 ns.

2.4.2. RIF-PAMAM complexes

As a result of the application of the "docking" approach described in Section 2.2, a set of RIF-PAMAM structures were obtained and ranked according to the number of RIF molecules and energy (see above). This procedure was performed for dendrimer structures appropriate for neutral and low pH. From the pool of structures with protonation states appropriate for neutral pH, the lowest energy structure corresponding to a complex involving 20 RIF

molecules and the G4-PAMAM was selected and labelled RIF_{20}-$PAMAM_N$, where the subscript N denotes "neutral". Analogously, a structure involving the same number of RIF molecules was chosen for low pH and labelled RIF_{20}-$PAMAM_L$. The topology file for the individual RIF molecule was generated using the same procedure as described above for the dendrimer, using the MKTOP program[95], the OPLS-AA force field.[86, 87] and the charges according to Ref.[96]. The systems RIF_{20}-$PAMAM_N$ and RIF_{20}-$PAMAM_L$ were energy minimized in vacuum using 5000 steepest descent followed by 5000 conjugate gradient cycles. Systems were then solvated with 18873 and 18891 water molecules, and neutralized with 64 and 126 Cl^- ions, respectively. A thorough and careful equilibration procedure was performed with position restraints on the dendrimer and on the RIF atoms, while the solvent and counterions were free to adapt to the RIF_{20}-PAMAM potential. This procedure was performed in a stepwise manner in which several sequential short simulations were employed. After each subsequential short simulation, the reference temperature was increased and the force constant of the restraining potential was decreased, until the system reached the desired reference temperature for the production run (310 K). From this point, the positional restraints were no longer employed and a 100 ns production run was carried out for each system.

3. Results and discussion

The results are organized as follows. Section 3.1 describes the experimental results concerning the determination of the number of RIF molecules per PAMAM dendrimer. Section 3.2 describes the results of the docking

procedure. Sections 3.3 and 3.4 discuss the results obtained from the molecular dynamics simulations in terms of the complexation on the structure of PAMAM and the stability of the RIF-PAMAM complexes, respectively.

3.1. Number of RIF molecules per complex

A maximum load of 20 RIF molecules per G4-PAMAM dendrimer was determined experimentally. There were two previous experiments reporting the association of RIF with a dendrimer, and both considered a polypropylenimine (PPI) dendrimer of 5^{th} generation.[25, 97] Kumar *et al.* have shown a maximum load of ∼37 RIF molecules per mannosylated G5-PPI dendrimer.[25] Due to the pronounced structural differences between PAMAM and PPI, and also due to the mannosylation, which affects the dendrimer size and properties, it is not straightforward to draw many conclusions from this comparison and a comparison between the complexation of the RIF-PAMAM complex and the complex of PAMAM with other drug may result in more insights. The drug ibuprofen, which has been highly studied in the context of drug-dendrimer complexes,[55, 98] will be considered in order to establish a comparative basis. Similarly to RIF, ibuprofen belongs to the class II pharmaceutical classification, which is characterized by high permeability and low solubility. The maximum number of 78 ibuprofen (molecular weight of 206.29 g mol^{-1}) molecules per G4-PAMAM was determined experimentally and was considered to be a high drug content.[98] It is four times larger than the number of RIF per G4-PAMAM, but note that RIF has a molecular weight of 822.94 g mol^{-1}, which is four times that of ibuprofen. Considering the molecular volume (calculated using 3V online[99]), RIF is about four times larger compared to ibuprofen, 1.086 and 0.276 nm^3, respec-

tively. Therefore, both drugs occupies similar volumes ($\sim$21 nm^3) within the cavities of PAMAM.

3.2. Docking of RIF molecules within the PAMAM cavities

Table 1 shows the success rates of the anchoring algorithm for 3 different dendrimer conformations, 3 different threshold distances and considering 2, 5, 10, 20 and 21 RIF molecules. All entries in this Table refer to values obtained using a Cauchy distribution, which was the one that lead to the highest success rates. With a threshold value of 1.5 nm, the success rate of anchoring 5 RIF molecules is about 65-80% and drops to about 20% for 10 RIF molecules. With such a small threshold value it is impossible to anchor a much higher load of RIF molecules. Considering a threshold value of 2.5 nm, the success rates of anchoring 5 and 10 RIF molecules increase to about 88-95% and 40-65%, respectively, and a small chance of finding a configuration with 20 RIF molecules, about 1%. At a threshold value of 3.5 nm, the success rates increase further and the encapsulation of 20 RIF molecules becomes more plausible, about 20-40% success rate. At this large threshold value, it is possible to observe a higher number of RIF for configurations 2 and 3. The encapsulation of 21 RIF molecules is possible at this threshold with a likelihood around 10-15%. However, it is important to mention that at a distance above $\sim$2 nm the RIF molecules are outside the radius of gyration of the G4-PAMAM. They are still considered to be encapsulated as the maximum dendrimer radius is about 3.5 nm, although they are interacting with the periphery of PAMAM. The success rate of docking 25 RIF molecules is zero for all 3 dendrimer conformations considered. The computational result suggests that a G4-PAMAM dendrimer is able to accommodate

approximately 20 molecules of RIF. Fig. 1c shows one of the configurations of the complex formed by 20 RIF molecules with G4-PAMAM and evidences a high density of RIF molecules. Fig. 1d shows one of the RIF molecules inside one of the cavities of G4-PAMAM.

3.3. PAMAM structural changes upon complex formation

In order to investigate the effects of complex formation on the dendrimer structure several radial distribution functions $g(r)$ were calculated for systems $PAMAM_N$, $PAMAM_L$, $RIF_{20}PAMAM_N$ and $RIF_{20}PAMAM_L$ (Figure 2). These systems correspond, respectively, to the PAMAM dendrimer in aqueous solution at neutral pH and low pH (subscripts N and L) and to the complex involving 20 RIF molecules and a PAMAM dendrimer at the same pH conditions.

Figure 2a shows the distributions of the water molecules relative to the dendrimer center of mass and reveals that the level of water penetration is significantly reduced comparing systems $RIF_{20}PAMAM_N$ with $PAMAM_N$ indicating that at neutral pH the RIF molecules partially replace the water molecules from the dendrimer cavities (black and green lines). On the other hand, comparing systems at low pH, the curves look very similar showing that systems $RIF_{20}PAMAM_L$ and $PAMAM_L$ have comparable hydration levels, which indicates that RIF molecules were expelled from the dendrimer cavities during the MD simulation of system $RIF_{20}PAMAM_L$. Figure 2b shows the distribution of Cl^- ions around the dendrimer center of mass. Comparing systems $RIF_{20}PAMAM_N$ and $PAMAM_N$ it is possible to note a big shift of the distributions indicating a higher anion penetration for the system $PAMAM_N$, which may also be attributed to a replacement of Cl^- ions by

RIF molecules upon complexation. Both systems at low pH, $RIF_{20}PAMAM_L$ and $PAMAM_L$, show a much more pronounced Cl^- penetration as a result of the protonated state of the tertiary amines. In addition, they show again very similar curves with the exception of a higher peak at very short distances for $PAMAM_L$. This difference at very short distance is attributed to the fact that $RIF_{20}PAMAM_L$ was still loaded with one RIF molecule at the end of the simulation (see Section 3.4). Figure 2c shows the distributions of the tertiary amine nitrogen atoms around the dendrimer center of mass. The peaks corresponding to the simulations at low pH are again very similar and evidence a high degree of order. The peak corresponding to the simulation of PAMAM at neutral pH, $PAMAM_N$, is much less ordered showing a more uniform probability distribution. In contrast, the simulation of the complex, $RIF_{20}PAMAM_N$, reveals a high degree of order and a shift of the peaks toward higher distances. This is an indicative that the complexation is accompanied by a swelling of the dendrimer interior. Figure 2d shows the distribution of the terminal amine nitrogen atoms with respect to the dendrimer center of mass. It is interesting to note that the distribution in the case of $RIF_{20}PAMAM_N$ is more similar to the ones corresponding to the systems simulated at low pH than to the simulation of $PAMAM_N$. The distribution reveals two peaks, one sharp peak just above 1 nm and a broad peak from $\sim$1.5 to $\sim$3.5 nm. This distribution starts at a higher distance ($\sim$0.8 nm) for system $RIF_{20}PAMAM_N$ compared to $PAMAM_N$ ($\sim$0.4 nm), again indicating a swelling of the internal dendrimer structure, but for higher distances ($\sim$2.5-3.5 nm) the distribution profile is similar for all 4 considered systems, which indicates that the internal swelling is not necessarily accompanied by

an increase in the maximum dendrimer radius.

The radius of gyration R_g was calculated for the four systems considering the last 10 ns of the simulations. $PAMAM_N$ shows a value of R_g of 1.96±0.02 nm compared to 2.03±0.02 nm for $RIF_{20}PAMAM_N$, evidencing a slight expansion upon complexation. This result is in line with the result of Barra *et al.*[74] that also reported a small size expansion due to drug-dendrimer encapsulation. The expansion due to the protonation of the internal amines was found to be more pronounced, 2.11±0.03 nm for $PAMAM_L$ compared to 1.96±0.02 nm for $PAMAM_N$.

3.4. RIF-PAMAM complex stability

The distances between the individual RIF molecules and the dendrimer center were monitored for systems at neutral and low pH and are shown in Figure 3. Considering the simulation at neutral pH, $RIF_{20}PAMAM_N$ (top panel), 19 RIF molecules remained well inside the dendrimer domain for the entire simulation time within a maximum distance of about 3.5 nm. One RIF molecule was released at the end of the simulation (∼90 ns). Therefore, at neutral pH, the simulation suggests a reasonably stable complex, which is consistent with the observed medially sustained release profile.[73] Considering the simulation at low pH, $RIF_{20}PAMAM_L$ (bottom panel), one can observe a completely different picture. The distances (19 out of 20) rise rapidly and almost simultaneously to values above 4 nm, indicating that the RIF molecules are rapidly expelled from the dendrimer cavities as the simulation proceeds. This is in line with previous studies that support that, at low pH, there is a triggered simultaneous release in contrast to a medially sustained release observed at neutral pH.[73, 100–102]

The $g(r)$ of center of mass of the RIF molecules with respect to the G4-PAMAM center of mass along with the $g(r)$ of the terminal amines (as in Figure 2d) were calculated considering the last 50 ns of the simulation trajectories of systems $RIF_{20}PAMAM_N$ and $RIF_{20}PAMAM_L$ and are displayed in Figure 4. Two important distances, the radius of gyration ($R_g =\sim 2$ nm) and the maximum radius ($R_{max} =\sim 3.5$ nm) are highlighted by thick dashed orange lines. In the inset, the $g(r)$ curves of center of mass of the RIF molecules with respect to the G4-PAMAM were not normalized so that the integrals correspond to the number of RIF molecules at a given distance. Considering the simulation at neutral pH, the RIF molecules lie within R_{max} and about ∼12-13 of them are present at distances below R_g. Therefore, about 2/3 of the RIF molecules are internally complexed with PAMAM, whereas about 1/3 of them interact with the dendrimer periphery. A similar behaviour has been reported by Barra *et al.*[74] in the study of the encapsulation of piroxicam (PRX) by a G3-PAMAM dendrimer. They have found a higher proportion (∼79% for PRX *vs.* ∼62% for RIF) of internally *vs.* externally complexed drug molecules, suggesting a stronger preference of PRX compared to RIF for internal complexation.

4. Conclusions

The association of a G4-PAMAM dendrimer with the antibiotic drug rifampicin (RIF) was investigated using experimental and computational methods aiming at determining the maximum RIF load per dendrimer and understanding the stability the drug release process at different pH conditions.

The maximum number of ∼20 RIF molecules per G4-PAMAM was determined experimentally. Based on this stoichiometry and relying on a computational multi-docking procedure, the starting configurations for molecular dynamics simulations were generated for the complexes at neutral and low pH. The MD simulations showed a reasonable stability for the complex at neutral pH, which is compatible with a medially sustained release also observed for other drug-dendrimer complexes. At low pH, the RIF molecules were rapidly and simultaneously expelled to the solvent bulk, agreeing with the observed triggered simultaneous release.[73] This pH switch is desirable in terms of the application of dendrimers as drug delivery systems towards acidic cellular structures such as the macrophage. One should keep in mind that this pH based vectorization may impose administration restrictions as for example in the case of oral administration due to the low pH of the stomach. Nevertheless, recent studies have shown that PAMAM dendrimers have potential for pulmonary inhalation,[103, 104] which may be highly advantageous in the case of tuberculosis treatment.

Acknowledgements

The authors would like to acknowledge the Brazilian agencies FAPERJ, CNPq and CAPES for financial support.

References

[1] A. Pawlowski, M. Jansson, M. Sköld, M.E. Rottenberg and G. Källenius, Tuberculosis and HIV co-infection, PLOS Pathogens 8 (2012) e1002464/1-e1002464/7.

[2] *Global Tuberculosis Report, WHO Press, World Health Organization, Geneva, Switzerland. Available at:* http://www.who.int/tb/publications/global_report/en/ (2013).

[3] H.M. Blumberg, W.J. Burman, R.E. Chaisson, C.L. Daley, S.C. Etkind, L.N. Friedman, P. Fujiwara, M. Grzemska, P.C. Hopewell, M.D. Iseman, R.M. Jasmer, V. Koppaka, R.I. Menzies, R.J. O'Brien, R.R. Reves, L.B. Reichman, P.M. Simone, J.R. Starke and A.A. Vernon, Treatment of tuberculosis, Am. J. Respir. Crit. Care Med. 167 (2003) 603-662.

[4] P. Blasi, A. Schoubben, S. Giovagnoli, C. Rossi and M. Ricci, Fighting tuberculosis: old drugs, new formulations, Expert Opin. Drug Deliv. 6 (2009) 977-993.

[5] W.J. Burman, K. Gallicano and C. Peloquin, Comparative pharmacokinetics and pharmacodynamics of the rifamycin antibacterials, Clin. Pharmacokinet. 40 (2001) 327-341.

[6] W.A. Petri Jr. Antimicrobial agents: drugs used in the chemotherapy of tuberculosis, Mycobacterium avium complex disease, and leprosy In: *Goodman, Gilman's: the pharmacological basis of therapeutics*; J.G. Hardman and L.E. Limbird, Eds.; New York, McGraw-Hill (2001); pp 1273-1294.

[7] B. Blomberg, S. Spinaci, B. Fourie and R. Laing, The rationale for recommending fixed-dose combination tablets fortreatment of tuberculosis, Bull. World Health Organ. 79 (2001) 61-79.

[8] N. Lounis and G. Roscigno, *In vitro* and *in vivo* activities of new rifamycin derivativesagainst mycobacterial infections, Curr. Pharm. Des. 10 (2004) 3229-3238.

[9] E. Maretti, T. Rossi, M. Bondi, M.A. Croce, M. Hanuskova, E. Leo, F. Sacchetti and V. Iannuccelli, Inhaled solid lipid microparticles to target alveolar macrophages for tuberculosis, Int. J. Pharm. 462 (2014) 74-82.

[10] S. Agrawal and R. Panchagnula, Implication of biopharmaceutics and pharmacokinetics of rifampicin in variable bioavailability from solid oral dosage forms, Biopharm. Drug Dispos. 26 (2004) 321-334.

[11] S. Agrawal, I. Singh, K.J. Kaur, S. Bhade, C.L. Kaul and R. Panchagnula, Bioequivalence trials of rifampicin containing formulations: extrinsic and intrinsic factors in the absorption of rifampicin., Pharm. Res. 50 (2004) 317-327.

[12] A. Sosnik, A.M. Carcaboso, R.J. Glisoni, M.A. Moretton and D.A. Chiappetta, New old challenges in tuberculosis: Potentially effective nanotechnologies in drug delivery, Adv. Drug Deliv. Rev. 62 (2010) 547-559.

[13] G.M. Sorokoumova, V.V. Vostrikov, A.A. Selishcheva, E.A. Rogozhkina, T.Yu.; Shvets Kalashnikova, Golyshevskaya V.I., Martynova V.I., Erokhin L.P., , Bacteriostatic activity and decomposition products of rifampicin in aqueous solution and liposomal composition, Pharm. Chem. J. 42 (2008) 475-478.

[14] C. Becker, J.B. Dressman, H.E. Junginger, S. Kopp, K.K. Midha, V.P. Shah, S. Stavchansky and D.M. Barends, Biowaiver monographs for immediate release solid oral dosage forms: rifampicin, J. Pharm. Sci. 98 (2009) 2252-2267.

[15] S. Qurrat-Ul-Ain; Sharma, G.K. Khuller and S.K. GARG, Alginate-based oral drug delivery system for tuberculosis: pharmacokinetics and therapeutic effects, J. Antimicrob. Chemother. 51 (2003) 931-938.

[16] N. Duran, M.A. Alvarenga, E.C. Silva, P.S. MELO and P.D. Marcato, Microencapsulation of antibiotic rifampicin in poly(3-hydroxybutyrate-co-3-hydroxyvalerate), Arch. Pharm. Res. 31 (2008) 1509-1516.

[17] M.L. Manca, G. Loy, M. Zaru, A.M. Fadda and S.G. Antimisiaris, Release of rifampicin from chitosan, PLGA and chitosan-coated PLGA microparticles, Coll. Surf. B 67 (2008) 166-170.

[18] K.N.A. Kumar, S.B. Ray, V. Nagaraja, , Encapsulation and release of rifampicin using poly(vinyl pyrrolidone)-poly(methacrylic acid) polyelectrolyte capsules, Mat. Sci. Eng. C 29 (2009) 2508-2513.

[19] K. Hirota, T. Hasegawa, T. Nakajima, H. Inagawa, C. Kohchi, G. Soma, K. Makino and H. Terada, Delivery of rifampicin-PLGA microspheres into alveolar macrophages is promising for treatment of tuberculosis, J. Control. Release 142 (2010) 339-346.

[20] I.I. Krasnyuk Jr., Effects of solid dispersions on the solubility of antibiotics, Pharm. Chem. J. 43 (2009) 226-229.

[21] P.K. Gaur, S. Mishra, V.B. Gupta, M.S. Rathod, S. Purohit and B.A. Savla, *In-situ* formation of liposome of rifampicin: better availability for better treatment, Curr. Drug Deliv. 6 (2009) 461-468.

[22] M.L. Manca, C. Sinico, A.M. Maccioni, O. Diez, A.M. Fadda and M. Manconi, Composition Influence on Pulmonary Delivery of Rifampicin Liposomes, Pharmaceutics 4 (2012) 590-606.

[23] S.K. Mehta, K.K. Bhasin, N. Mehta and S. Dham, Behavior of rifampicin in association with β-cyclodextrin in aqueous media: a spectroscopic and conductometric study, Coll. Polym. Sci. 283 (2005) 532-538.

[24] J.S. Patil and S. Suresh, Physicochemical characterization, *in vitro* release and permeation studies of respirable rifampicin-cyclodextrin inclusion complexes, Indian J. Pharm. Sci. 71 (2009) 638-643.

[25] P.V. Kumar, A. Asthana, T. Dutta and N.K. Jain, Intracellular macrophage uptake of rifampicin loaded mannosylated dendrimers, J. Drug Target. 14 (2006) 546-556.

[26] G.M. Dykes, Dendrimers: a review of their appeal and applications, J. Chem. Technol. Biotechnol. 76 (2001) 903-918.

[27] Z. Yang, B. Xu, J. He, L. Xue, Q. Guo, H. Xia and W. Tian, Solution-processable and thermal-stable triphenylamine-based dendrimers with truxene cores as hole-transporting materials for organic light-emitting devices, Org. Electronics 10 (2009) 954-959.

[28] E. Bustos and L.A. Godinez, Modified surfaces with nano-structured composites of prussian blue and dendrimers. New Materials for Advanced Electrochemical Applications, Int. J. Electrochem. Sci. 6 (2011) 1-36.

[29] D. Tuerp, N. Thi-Thanh-Tam, M. Baumgarten and K. Muellen, Uniquely versatile: nano-site defined materials based on polyphenylene dendrimers, New J. Chem. 36 (2012) 282-298.

[30] Z. Shi, S. Hau, J. Luo, T.-D. Kim, N.M. Tucker, J.-W. Ka, H. Sun, A. Pyajt, L. Dalton, A. Chen and A.K.Y. Jen, Highly efficient diels-alder crosslinkable electro-optic dendrimers for electric-field sensors, Adv. Funct. Mater. 17 (2007) 2557-2563.

[31] M.R. Harpham, O. Suezer, C.-Q. Ma, P. Baeuerle, T. Goodson, , Thiophene Dendrimers as Entangled Photon Sensor Materials, J. Am. Chem. Soc. 131 (2009) 973-979.

[32] A.-M. Caminade, B. Delavaux-Nicot, R. Laurent and J.-P. Majoral, Sensitive Sensors Based on Phosphorus Dendrimers, Curr. Org. Chem. 14 (2010) 500-515.

[33] J. Guerra, M. Antonia Herrero, B. Carrion, F.C. Perez-Martinez, M. Lucio, N. Rubio, M. Meneghetti, M. Prato, V. Cena and E. Vazquez, Carbon nanohorns functionalized with polyamidoamine dendrimers as efficient biocarrier materials for gene therapy, Carbon 50 (2012) 2832-2844.

[34] Z. Cheng, D.L.J. Thorek and A. Tsourkas, Porous polymersomes with encapsulated Gd-Labeled dendrimers as highly efficient MRI contrast agents, Adv. Funct. Mat. 19 (2009) 3753-3759.

[35] W.C. Floyd, P.J. Klemm III, D.E. Smiles, A.C. Kohlgruber, V.C. Pierre, J.L. Mynar, J.M.J. Frechet and K. N. Raymond, Conjugation effects of various linkers on Gd(III) MRI contrast agents with dendrimers: Optimizing the hydroxypyridinonate (HOPO) ligands with nontoxic, degradable esteramide (EA) dendrimers for high relaxivity, J. Am. Chem. Soc. 133 (2011) 2390-2393.

[36] D.K. Keum, K. Naka and Y. Chujo, Effect of anionic polyamidoamine dendrimers on the crystallization of calcium carbonate by delayed addition method, Bull. Chem. Soc. Japan 76 (2003) 1687-1691.

[37] S.-J. Yan, Z.-H. Zhou, F. Zhang, S.-P. Yang, L.-Z. Yang and X.-B. Yu, Effect of anionic PAMAM with amido groups starburst dendrimers on the crystallization of Ca-10(PO4)(6)(OH)(2)) by hydrothermal method, Mat. Chem. Phys. 99 (2006) 164-169.

[38] A. Mahajan, S. R. Chhabra and W. C. Chan, Resin-bound dendrimers as high loading supports for solid phase chemistry, Tetrahedron Lett. 40 (1999) 4909-4912.

[39] G. Zaupa, L. J. Prins and P. Scrimin, Resin-supported catalytic dendrimers as multivalent artificial metallonucleases, Bioorg. Med. Chem. Lett. 19 (2009) 3816-3820.

[40] M. P. Kapoor, H. Kuroda, M. Yanagi, H. Nanbu and L. R. Juneja, Catalysis by Mesoporous Dendrimers, Top. Catal. 52 (2009) 634-642.

[41] D. Astruc, Palladium catalysis using dendrimers: molecular catalysts versus nanoparticles, Tetrahedron Asymmetry 21 (2010) 1041-1054.

[42] D. Astruc, Electron-transfer processes in dendrimers and their implication in biology, catalysis, sensing and nanotechnology, Nat. Chem. 4 (2012) 255-267.

[43] K. Borowska, B. Laskowska, A. Magon, B. Mysliwiec, M. Pyda and S. Wolowiec, PAMAM dendrimers as solubilizers and hosts for 8-methoxypsoralene enabling transdermal diffusion of the guest, Int. J. Pharm. 398 (2010) 185-189.

[44] S. Svenson and D.A. Tomalia, Dendrimers in biomedical applicationsreflections on the field, Adv. Drug Deliv. Rev. 57 (2005) 2106-2129.

[45] B. Devarakonda, R. A. Hill, W. Liebenberg, M. Brits and M. M. de Villiers, Comparison of the aqueous solubilization of practically insoluble niclosamide by polyamidoamine (PAMAM) dendrimers and cyclodextrins, Int. J. Pharm. 304 (2005) 193-209.

[46] S. Svenson and A. S. Chauhan, Dendrimers for enhanced drug solubilization, Nanomedicine 3 (2008) 679-702.

[47] S. Svenson, Dendrimers as versatile platform in drug delivery applications, Eur. J. Pharm. Biopharm. 71 (2009) 445-462.

[48] J. Hu, Y. Su, H. Zhang, T. Xu and Y. Cheng, Design of interior-functionalized fully acetylated dendrimers for anticancer drug delivery, Biomaterials 32 (2011) 9950-9959.

[49] J. Lim and E.E. Simanek, Triazine dendrimers as drug delivery systems: From synthesis to therapy, Adv. Drug Deliv. Rev. 64 (2012) 826-835.

[50] J. Liu, W.D. Gray, M.E. Davis and Y. Luo, Peptide- and saccharide-conjugated dendrimers for targeted drug delivery: A concise review, Interface Focus 2 (2012) 307-324.

[51] S. Sadekar and H. Ghandehari, Transepithelial transport and toxicity of PAMAM dendrimers: Implications for oral drug delivery, Adv. Drug Deliv. Rev. 64 (2012) 571-588.

[52] A. Vergara-Jaque, J. Comer, L. Monsalve, F.D. González-Nilo and C. Sandoval, Computationally efficient methodology for atomic-level characterization of dendrimer-drug complexes: a comparison of amine- and acetyl-terminated PAMAM, J. Phys. Chem. B 117 (2013) 6801-6813.

[53] R. Esfand and D.A. Tomalia, Poly(amidoamine) (PAMMAM) dendrimers: from biomimicry to drug delivery and biomedical applications, Drug Discovery Today 6 (2001) 427-36.

[54] S. Hong, A.U. Bielinska, A. Mecke, B. Keszler, J.L. Beals, X. Shi, L. Balogh, B.G. Orr, J.R. Baker Jr. and M.M. Banaszak Holl, Interaction of poly(amidoamine) dendrimers with supported lipid bilayers and cells: hole formation and the relation to transport, Bioconjug. Chem. 15 (2004) 774-782.

[55] I. Tanis and K. Karatasos, Association of a weakly acidic anti-inflammatory drug (ibuprofen) with a poly(amidoamine) dendrimer as studied by molecular dynamics simulations, J. Phys. Chem. B 113 (2009) 10984-10993.

[56] A. Åkesson, T.K. Lind, R. Barker, A. Hughes and M. Cárdenas, Unraveling dendrimer translocation across cell membrane mimics, Langmuir 28 (2012) 13025-13033.

[57] J. Caballero, H. Poblete, C. Navarro and J.H. Alzate-Morales, Association of nicotinic acid with a poly(amidoamine) dendrimer studied by molecular dynamics simulations, J. Mol. Graph. Model. 39 (2013) 71-78.

[58] D.A. Tomalia, A.M. Naylor and W.A. Goddard III, Starburst dendrimers: molecular-Level control of size, shape, surface chemistry, topology, and flexibility from atoms to macroscopic matter, Angew. Chem. Int. Ed. 29 (2003) 138-175.

[59] S.-T. Lin, P.K. Maiti and W.A. Goddard III, Dynamics and thermodynamics of water in PAMAM dendrimers at subnanosecond time scales, J. Phys. Chem. 109 (2005) 8663-8672.

[60] W.-D. Tian and Y.-Q. Ma, Molecular dynamics simulations of a charged dendrimer in multivalent salt solutio, J. Phys. Chem. B 113 (2009) 13161-13170.

[61] P.K. Maiti, Y. Li, T. Cagin and W.A. Goddard III, Structure of polyamidoamide dendrimers up to limiting generations: A mesoscale description, J. Chem. Phys. 130 (2009) 144902/1-144902/10.

[62] J. Aumanen, T. Kesti, V. Sundström, G. Teobaldi, F. Zerbetto, N. Werner, G. Richardt, J. van Heyst, F. Vögtle and J. Korppi-Tommola, Internal dynamics and energy transfer in dansylated POPAM dendrimers and their eosin complexes, J. Phys. Chem. B 114 (2010) 1548-1558.

[63] Y. Li and T. Hou, Computational Simulation of Drug Delivery at Molecular Level, Curr. Med. Chem. 17 (2010) 4482-4491.

[64] W.-D. Tian and Y.-Q. Ma, Insights into the endosomal escape mechanism via investigation ofdendrimermembrane interactions, Soft Matter 8 (2012) 6378-6384.

[65] B. Nandy, P.K. Maiti and A. Bunker, Force biased molecular dynamics simulation study of effect ofdendrimer generation on interaction with DNA, J. Chem. Theory Comput. 9 (2012) 722-729.

[66] W.-d. Tian and Y.-q. Ma, Theoretical and computational studies of dendrimers as delivery vectors, Chem. Soc. Rev. 42 (2013) 705-727.

[67] M. Mills, B.G. Orr, M.M.B. Holl and I. Andricioaei, Attractive hydration forces in DNA-dendrimer interactions on the nanometer scale, J. Phys. Chem. B 117 (2013) 973-981.

[68] M.P. Allen and D.J. Tildesley, *Computer simulation of liquids*, Oxford University Press, New York, USA (1987).

[69] W.F. van Gunsteren and H.J.C. Berendsen, Computer simulation of molecular dynamics: Methodology, applications and perspectives in chemistry, Angew. Chem. Int. Ed. 29 (1990) 992-1023.

[70] W.F. van Gunsteren, D. Bakowies, R. Baron, I Chandrasekhar, M. Christen, X. Daura, P. Gee, D.P. Geerke, A. Glättli, P.H. Hünenberger, M.A. Kastenholz, C. Oostenbrink, M. Schenk, D. Trzesniak, N.F.A. van der Vegt and H.B. Yu, Biomolecular modelling: goals, problems, perspectives, Angew. Chem. Int. Ed. 45 (2006) 4064-4092.

[71] H.J.C. Berendsen, *Simulating the physical world*, Cambridge University Press, Cambridge, UK (2007).

[72] V. Maingi, M.V.S. Kumar and P.K. Maiti, PAMAM DendrimerDrug Interactions: Effect of pH on the Binding and Release Pattern, J. Phys. Chem. B 116 (2012) 4370-4376.

[73] V. Jain, V. Maingi, P.K. Maiti and P.V. Bharatam, Molecular dynamics simulations of PPI dendrimer-drug complexes, Soft Matter 9 (2013) 6482-6496.

[74] P.A. Barra, L.F. Barraza, V.A. Jiménez, J.A. Gavin and J.B. Alderete, Drug-dendrimer supramolecular complexation studied from molecular dynamics simulations and NMR spectroscopy, Struct. Chem. 25 (2014) 1443-1455.

[75] V. Law, C. Knox, Y. Djoumbou, T. Jewison, A.C. Guo, Y. Liu, A. Maciejewski, D. Arndt, M. Wilson, V. Neveu, A. Tang, G. Gabriel, C. Ly, S. Adamjee, Z.T. Dame, B. Han, Y. Zhou and D.S. Wishart, DrugBank 4.0: shedding new light on drug metabolism, Nucleic Acids Res. 42 (2014) D1091-D1097.

[76] C.S. de Magalhães, H.J.C. Barbosa and L.E. Dardenne, A genetic algorithm for the ligand-protein docking problem, Genet. Mol. Biol. 4 (2004) 605-610.

[77] S.F. Sousa, P.A. Fernandes and M.J. Ramos, Protein-ligand docking: Current status and future challenges, Proteins: Struct. Funct. Bioinf. 65 (2006) 15-26.

[78] Z. Zsoldos, D. Reid, A. Simon, S.B. Sadjad and A.P. Johnson, eHiTS: A new fast, exhaustive flexible ligand docking system, J. Mol. Graph. Model. 26 (2007) 198-212.

[79] S.-Y. Huang and X. Zou, Advances and challenges in protein-ligand docking, Int. J. Mol. Sci. 11 (2010) 3016-3034.

[80] S.L. Mayo, B.D. Olafson and W.A. Goddard III, DREIDING: A Generic Force Field for Molecular Simulation, J. Phys. Chem. 94 (1990) 8897-8909.

[81] M.J. Frisch, G.W. Trucks, H.B. Schlegel, G.E. Scuseria, M.A. Robb, J.R. Cheeseman, J.A. Montgomery Jr., T. Vreven, K.N. Kudin, J.C. Burant, J.M. Millam, S.S. Iyengar, J. Tomasi, V. Barone, B. Mennucci, M. Cossi, G. Scalmani, N. Rega, G.A. Petersson, H. Nakatsuji, M. Hada, M. Ehara, K. Toyota, R. Fukuda, J. Hasegawa, M. Ishida, T. Nakajima, Y. Honda, O. Kitao, H. Nakai, M. Klene, X. Li, J.E. Knox, H.P. Hratchian, J.B. Cross, V. Bakken, C. Adamo, J. Jaramillo, R. Gomperts, R.E. Stratmann, O. Yazyev, A.J. Austin, R. Cammi, C. Pomelli, J.W. Ochterski, P.Y. Ayala, K. Morokuma, G.A. Voth, P. Salvador, J.J. DAnnenber, V.G. Zakrzewski, S. Dapprich, A.D. Daniels, M.C. Strain, O. Farkas, D.K. Malick, A.D. Rabuck, K. Raghavachari, J.B. Foresman, J.V. Ortiz, Q. Cui, A.G. Baboul, S. Clifford, J. Cioslowski, B.B. Stefanov, G. Liu, A. Liashenko, P. Piskorz, I. Komaromi, R.L. Martin, D.J. Fox, T. Keith, M.A. Al-laham, C.Y. Peng, A. Nanayakkara, M. Challacombe, P.M.W. Gill, B. Johnson, W. Chen, M.W. Wong, C. Gonzalez and J.A. Pople, *Gaussian 03, Revision D.0*, Gaussian, Inc., Wallingford CT (2004).

[82] H.J.C. Berendsen, D. van der Spoel and R. van Drunen, GROMACS: A message-passing parallel molecular dynamics implementation, Comput. Phys. Commun. 91 (1995) 43-56.

[83] E. Lindahl, B. Hess and D. van der Spoel, GROMACS 3.0: A package for molecular simulation and trajectory analysis, J. Mol. Model. 7 (2001) 306-317.

[84] D. van der Spoel, E. Lindahl, B. Hess, G. Groenhof, A.E. Mark and H.J.C. Berendsen, GROMACS: Fast, flexible, and free, J. Comput. Chem. 26 (2005) 1701-1718.

[85] B. Hess, C. Kutzner, D. van der Spoel and E. Lindahl, GROMACS 4: Algorithms for highly efficient, load-balanced, and scalable molecular simulation, J. Chem. Theory Comput. 4 (2008) 435-447.

[86] W.L. Jorgensen, D.S. Maxwell and J. Tirado-Rives, Development and testing of the OPLS all-atom force field on conformational energetics and properties of organic liquids, J. Am. Chem. Soc. 118 (1996) 11225-11236.

[87] G.A. Kaminski, R.A. Friesner, J. Tirado-Rives and W.L. Jorgensen, Evaluation and reparametrization of the OPLS-AA force field for proteins via comparison with accurate quantum chemical calculations on peptides, J. Phys. Chem. B 105 (2001) 6474-6487.

[88] W.L. Jorgensen, J. Chandrasekhar, J.D. Madura, R.W. Impey and M.L. Klein, Comparison of simple potential functions for simulating liquid water, J. Chem. Phys. 79 (1983) 926-935.

[89] R.W. Hockney, The potential calculation and some applications, Methods Comput. Phys. 9 (1970) 135-211.

[90] B. Hess, H. Bekker, H.J.C. Berendsen and J.G.E.M. Fraaije, LINCS : A linear constraint solver for molecular simulations, J. Comput. Chem. 18 (1997) 1463-1472.

[91] H.J.C. Berendsen, J.P.M. Postma, W.F. van Gunsteren, A. di Nola and J.R. Haak, Molecular dynamics with coupling to an external bath, J. Chem. Phys. 81 (1984) 3684-3690.

[92] U. Essmann, L. Perera, M.L. Berkowitz, T. Darden, H. Lee and L.G. Pedersen, A smooth particle mesh Ewald method, J. Chem. Phys. 103 (1995) 8577-8593.

[93] *HyperChem(TM) Professional 7.51, Hypercube, Inc., 1115 NW 4th Street, Gainesville, Florida 32601, USA. Available at:* http://www.hyper.com.

[94] D. Cakara, J. Kleimann and M. Borkovec, Microscopic protonation equilibria of poly(amidoamine) dendrimers from macroscopic titrations, Macromolecules 36 (2003) 4201-4207.

[95] A.A.S.T. Ribeiro, B.A.C. Horta and R.B. de Alencastro, MKTOP: a program for automatic construction of molecular topologies, J. Braz. Chem. Soc. 19 (2008) 1433-1435.

[96] R.H. Henchman and J.W. Essex, Generation of OPLS-like charges from molecular electrostatic potential using restraints, J. Comput. Chem. 20 (1999) 483-398.

[97] B.V. Manalan, P. Kolavennu, A.E. Prabahar, R.R. Nadendla and K. Manukonda, Dendritic nanoparticulated carriers for the delivery of anti tuberculosis bioactives, Int. J. Biol. Pharm. Res. 5 (2014) 913-920.

[98] P. Kolhe, E. Misra, R.M. Kannan, S. Kannan and M. Lieh-Lai, Drug complexation, in vitro release and cellular entry of dendrimers and hyperbranched polymers, Int. J. Pharm. 259 (2003) 143-160.

[99] N.R. Voss and M. Gerstein, 3V: cavity, channel and cleft volume calculator and extractor, Nucleic Acids Res. 38 (2010) W555-W562.

[100] G. Pistolis, A. Malliaris, D. Tsiourvas and C.M. Paleos, Poly(propyleneimine) dendrimers as pH-sensitive controlled-release systems, Chem. Eur. J. 5 (1999) 1440-1444.

[101] B. Devarakonda, D.P. Otto, A. Judefeind, R.A. Hill and M.M. de Villiers, Effect of pH on the solubility and release of furosemide from polyamidoamine (PAMAM) dendrimer complexes, Int. J. Pharm. 345 (2007) 142-153.

[102] R.K. Tekade, T. Dutta, V. Gajbhiye and N.K. Jain, Exploring dendrimer towards dual drug delivery: pH responsive simultaneous drug-release kinetics, J. Microencapsulation 26 (2009) 287-296.

[103] M. Nasr, M. Najlah, A. D'Emanuele and A. Elhissi, PAMAM dendrimers as aerosol drug nanocarriers for pulmonary delivery via nebulization, Int. J. Pharm. 461 (2014) 242-250.

[104] Z. Dong, K.A. Hamid, Y. Gao, Katsumi Lin. Y., Sakane H., Yamamoto T., , Polyamidoamine dendrimers can improve the pulmonary absorption of insulin and calcitonin in rats, J. Pharm. Sci. 100 (2011) 1866-1878.

5. Figures

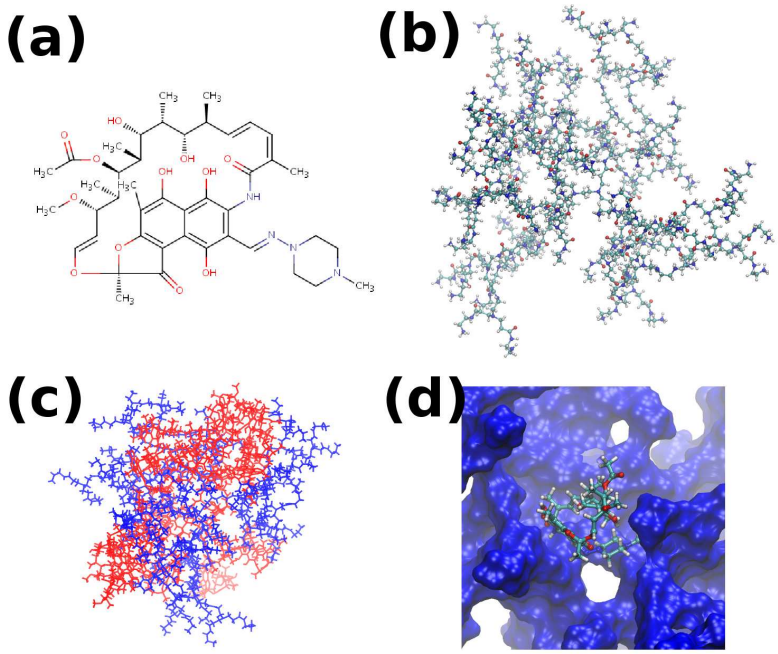

Figure 1: Graphical representations of: (a) structural formula of rifampicin; (b) three-dimensional structure of a G4-PAMAM dendrimer; (c) three-dimensional structure of one of the configurations generated by the docking procedure for the complex formed by 20 RIF (red) molecules and one G4-PAMAM (blue) and (d) a view of one of the RIF molecules in ball and stick representation inside one of the cavities of the dendrimer represented by a blue contour surface.

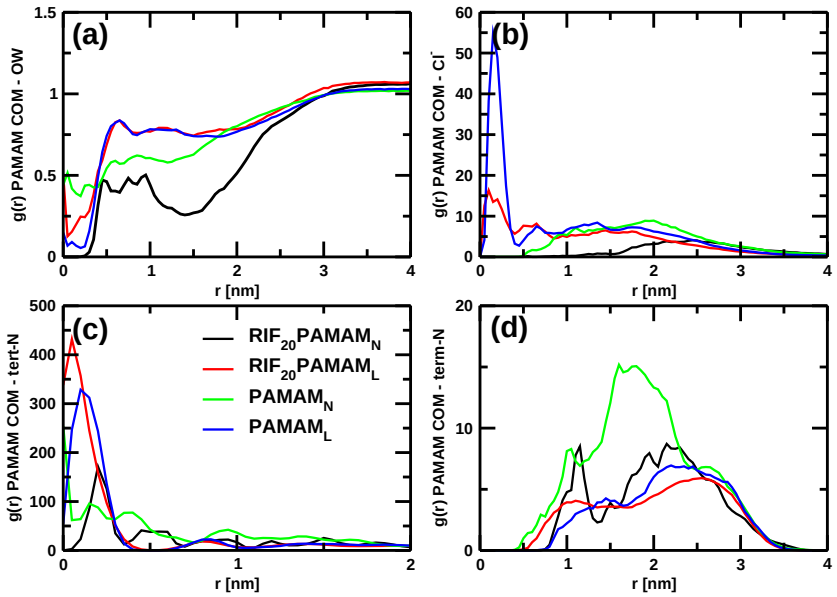

Figure 2: Radial distribution function ($g(r)$) curves calculated with respect to the PAMAM dendrimer center of mass and normalized according to density and volume. (a) oxygen atom (OW) of water molecules; (b) Cl^- counterions; (c) PAMAM tertiary nitrogen atoms and (d) PAMAM terminal nitrogen atoms.

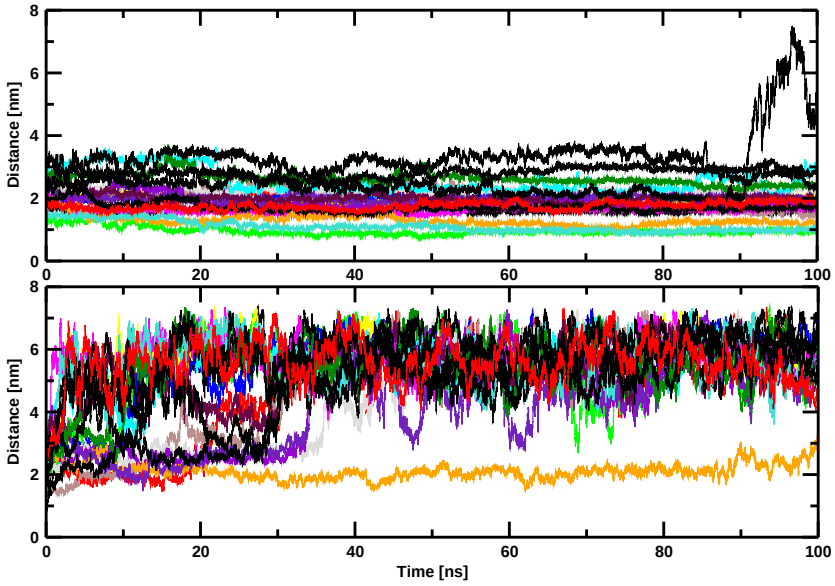

Figure 3: Time series of the distances between the center of mass of the RIF molecules and the dendrimer center of mass. Top and bottom panels refer, respectively, to the simulations at neutral and low pH conditions. Each line correspond to an individual RIF molecule.

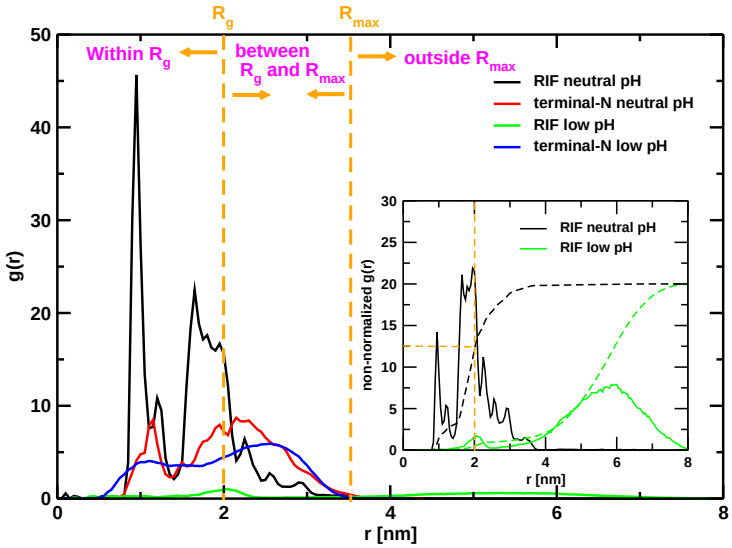

Figure 4: In the outer panel, the radial distribution function ($g(r)$) curves calculated with respect to the PAMAM dendrimer center of mass (COM) and normalized according to density and volume. The black and green lines refer to the $g(r)$ of the COM of RIF molecules around the dendrimer COM, whereas the red and blue lines correspond to the $g(r)$ of the terminal nitrogen atoms around the dendrimer COM (same as in Figure 2 panel (d)). The dashed orange lines refer to the distances corresponding to the radius of gyration (R_g) and to the maximum dendrimer radius (R_{max}). In the inset, the non-normalized $g(r)$ of the COM of RIF molecules around the dendrimer COM are shown with continuous lines and the dashed lines are the corresponding integration curves.

6. Tables

Table 1

Success rates of the algorithm for generating initial configurations with refinement based on a Cauchy distribution. The results are shown for 2, 5, 10, 20 and 21 molecules, with threshold distances (R_t) of 1.5, 2.5 and 3.5 nm and for three time-uncorrelated dendrimer conformations obtained from a previous MD simulation.

		Success rate		
R_t [nm]	Num. molecules	Conf. 1 [%]	Conf. 2 [%]	Conf. 3 [%]
≤ 1.5	2	95.5	100.0	98.2
	5	64.1	78.7	79.1
	10	22.3	19.2	23.0
	20	–	–	–
≤ 2.5	2	100.0	100.0	100.0
	5	88.6	94.6	92.2
	10	41.1	65.2	59.7
	20	–	1.4	0.4
	21	–	–	–
≤ 3.5	2	100.0	100.0	100.0
	5	95.4	97.4	98.8
	10	81.5	84.2	84.6
	20	21.1	37.1	39.6
	21	–	11.1	14.2
	25	–	–	–